Volume 60
Number 16
25 February 2024
Pages 2105–2250

ChemComm

Chemical Communications

rsc.li/chemcomm

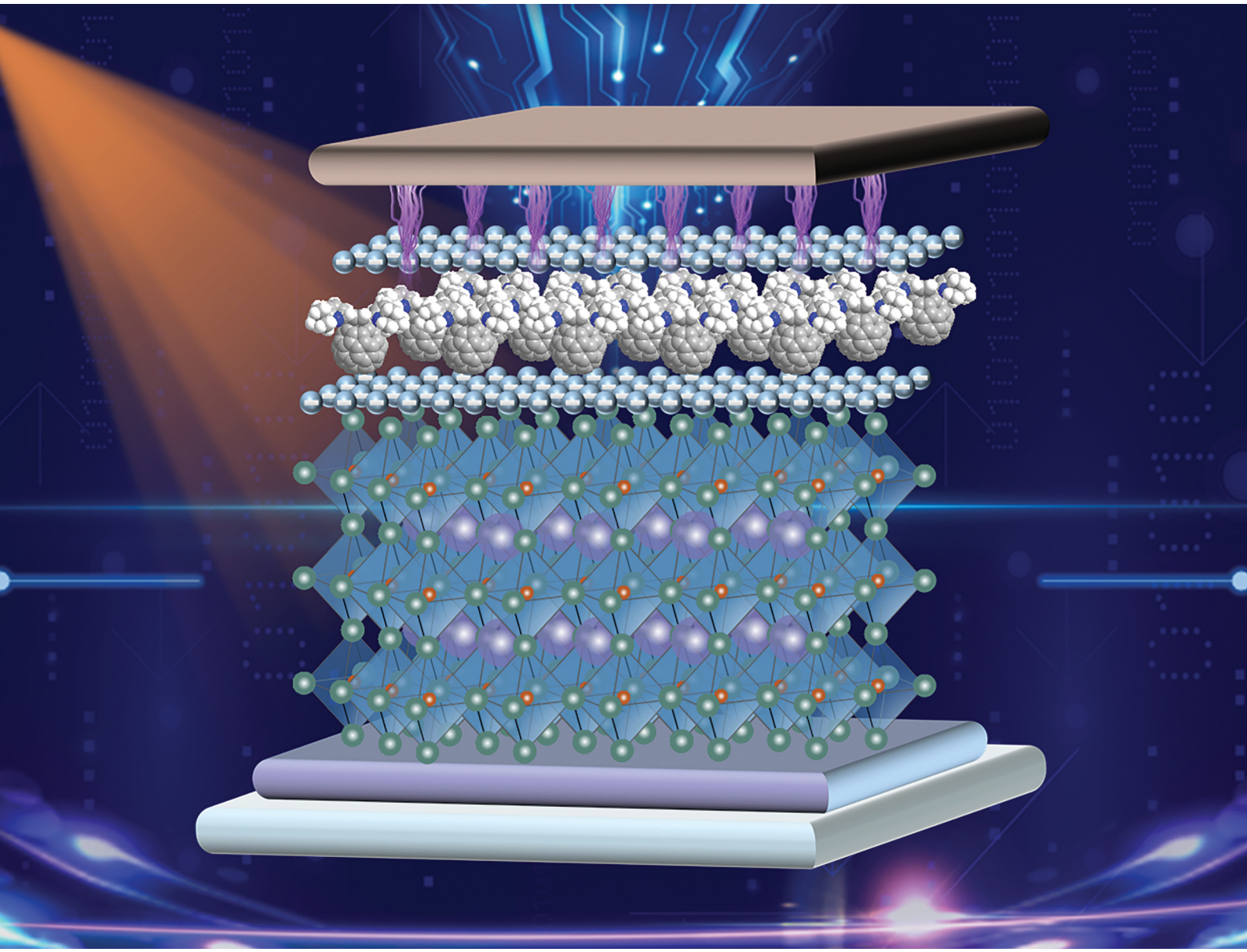

ISSN 1359-7345

ROYAL SOCIETY OF CHEMISTRY

COMMUNICATION

Yasujiro Murata, Atsushi Wakamiya *et al.*
An open-cage bis[60]fulleroid as an electron transport material for tin halide perovskite solar cells

60 YEARS ANNIVERSARY

ChemComm

COMMUNICATION

View Article Online
View Journal | View Issue

Cite this: *Chem. Commun.*, 2024, **60**, 2172

Received 29th November 2023,
Accepted 22nd January 2024

DOI: 10.1039/d3cc05843c

rsc.li/chemcomm

An open-cage bis[60]fulleroid as an electron transport material for tin halide perovskite solar cells†

Wentao Liu, ‡ Guanglin Huang, ‡ Chien-Yu Chen,‡ Tiancheng Tan, Harata Fuyuki, Shuaifeng Hu, Tomoya Nakamura, Minh Anh Truong, Richard Murdey, Yoshifumi Hashikawa, Yasujiro Murata * and Atsushi Wakamiya *

An open-cage bis[60]fulleroid (OC) was applied as an electron transport material (ETM) in tin (Sn) halide perovskite solar cells (PSCs). Due to the reduced offset between the energy levels of Sn-based perovskites and ETMs, the power conversion efficiency (PCE) of Sn-based PSCs with OC reached 9.6% with an open-circuit voltage (V_{OC}) of 0.72 V. Additionally, OC exhibited superior thermal stability and provided 75% of the material without decomposition after vacuum deposition. The PSC using vacuum-deposited OC as the ETM could afford a PCE of 7.6%, which is a big leap forward compared with previous results using vacuum-deposited fullerene derivatives as ETMs.

Metal halide perovskite solar cells have been widely regarded as one of the most promising candidates to replace silicon solar cells, owing to their PCE of over 26% achieved with the low-cost solution-processed neat lead (Pb) perovskites.[1] However, Pb involved in the most efficient PSCs is notorious for its toxicity, which may hinder the widespread application of this technology.[2,3] In this regard, Sn-based perovskites have attracted increasing interest due to their similar photophysical properties as Pb-based perovskites and environmentally benign properties.[4–8] Despite their great potential, the highest reported PCE of Sn-based PSCs is currently lower than 15%,[9] far below their theoretical limit of over 30%.[10]

One of the biggest challenges for Sn-based PSCs is the considerable V_{OC} loss, primarily induced by the energy level mismatch between the conduction band minimum of Sn-based perovskites and the lowest unoccupied molecular orbital (LUMO) levels of traditional fullerene ETMs, *i.e.*, C_{60}.[11] Thus, it is highly desirable to develop ETMs with shallower LUMO levels. Introduction of functional groups onto the C_{60} cages is an effective way to adjust the LUMO level of fullerene derivatives.[12,13] Phenyl-C_{61}-butyric acid methyl ester (PCBM) and indene-C_{60} bisadduct (ICBA) (Fig. 1) are typical mono and bis-functionalized fullerene derivatives that have been used to reduce V_{OC} loss in Sn-based PSCs.[11] However, bis- and multiple-additions often yield isomers possessing similar polarity, which requires extensive recycling using high-performance liquid chromatography (HPLC) for separation and leads to low yields.[14] Moreover, as each isomer exhibits both different energy levels and varied quality on the films, it is difficult to distinguish the respective effects when using the mixture as an ETM.[15,16]

Open-cage fullerene derivatives[17–19] enable flexible adjustment of their energy levels by the selective modifications, which results in a controlled functionalization degree as opposed to conventional C_{60} derivatization generating a complex mixture of isomers. These characteristics make them promising ETMs in PSCs. Nevertheless, there are limited reports on applying them in PSCs, except for a few reports on organic photovoltaics[20–22] and Pb-halide solar cells.[23] Herein, we focus on an open-cage

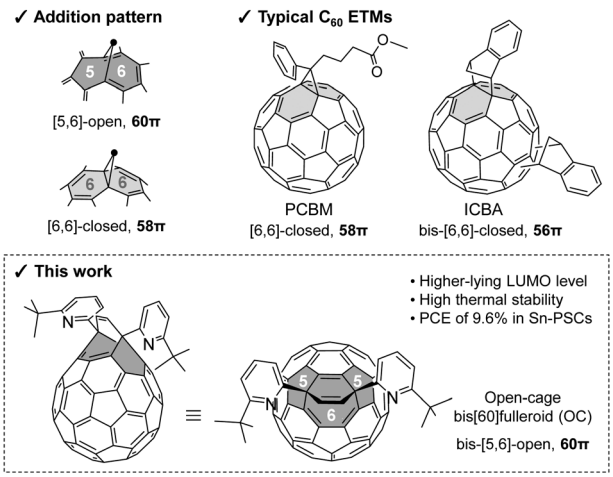

Fig. 1 Structures of PCBM, ICBA, and OC.

Institute for Chemical Research, Kyoto University, Uji, Kyoto 611-0011, Japan.
E-mail: yasujiro@scl.kyoto-u.ac.jp, wakamiya@scl.kyoto-u.ac.jp

† Electronic supplementary information (ESI) available. See DOI: https://doi.org/10.1039/d3cc05843c

‡ These three authors contributed equally.

bis[60]fulleroid (OC) (Fig. 1), which possesses two [5,6]-open structures (the bond between hexagon and pentagon is cleaved) with retaining the intact 60π system of parent C_{60}. This is different from PCBM, which features a [6,6]-closed structure (the addend is attached on a bond between hexagons) with a 58π system. Although the use of [5,6]-open PCBM has been hampered due to a rapid chemical transformation into a [6,6]-closed analogue,[24–27] bis-[5,6]-open OC is thermally stable even at 260 °C without showing any isomerism owing to the disfavoured generation of an intermediate having two [5,6]-closed structures at the *cis*-1 disposition in close proximity.[28,29] Furthermore, bis-functionalization of C_{60} (bis-[6,6]PCBM and ICBA) usually leads to a greater V_{OC}, owing to the higher-lying LUMO level.[30] Therefore, the bis-[5,6]-open structure in the OC is highly attractive for application in PSCs as the ETM. In this work, the resultant Sn-based PSCs using OC as ETMs presented a PCE of 9.6% with a V_{OC} of 0.72 V, comparable with those based on ICBA and significantly higher than those of PCBM. We also explored the vacuum-deposited OC to be an ETM layer, which afforded a PCE of 7.6% in PSCs.

Target compound OC was synthesized according to a previous report[31] and the purity was confirmed by ^{1}H NMR and MS analysis (Fig. S1 and S2, ESI†), with no observations of unreacted C_{60} nor solvent molecules in the sample. To compare the electronic properties of OC with commercial ETMs, *i.e.*, PCBM and ICBA, we performed UV-vis measurements (Fig. 2a). From the spectra, OC was found to show similar absorption behaviour to PCBM owning to the (pseudo) C_S symmetry while ICBA exhibits stronger absorption, especially at the UV and visible region, reflecting its lower symmetry.[20] Then, we conducted cyclic voltammetry (CV) in *o*-dichlorobenzene (ODCB) using Fc/Fc^+ as an internal standard (Fig. 2b). The first reduction potential of OC (−1.23 V) showed a cathodic shift relative to PCBM of −1.16 V and an anodic shift relative to ICBA of −1.33 V, consistent with the tendency of the LUMO levels calculated at the B3LYP-D3/6-31G(d,p) level: −2.93 eV (OC), −2.99 eV (PCBM), and −2.92 eV (ICBA, isomer *trans*-1). Although OC has a 60π system, the LUMO level is much higher than that of C_{60} (−3.22 eV). This is caused by two sp^3 units working as effective electron-donating groups. Therefore, the LUMO level of OC became comparable to that of ICBA but higher than that of PCBM. This MO level modification is different from those for conventional fullerene derivatives whose MO levels are mainly governed by the functionalization degree (such as mono, bis, and tris).

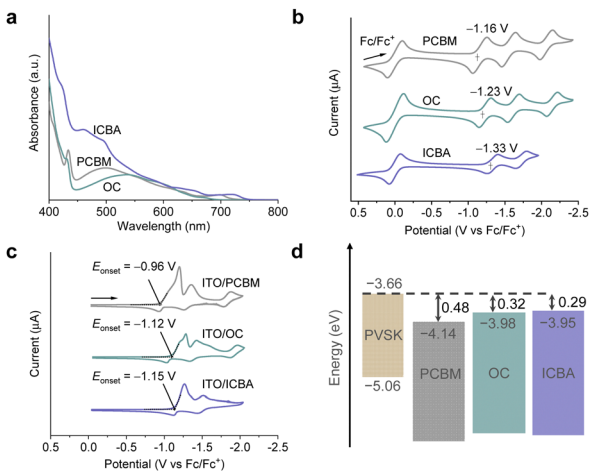

Fig. 2 (a) UV-vis absorption spectra of PCBM, OC, and ICBA (50 μM). (b) Cyclic voltammograms (CV) of PCBM, OC, and ICBA in ODCB (1.0 mM). (c) CV for spin-coated PCBM, OC, and ICBA films in acetonitrile. (d) Energy level diagrams of $PEA_{0.15}FA_{0.85}SnI_3$ and PCBM, OC, and ICBA films. PVSK denotes $PEA_{0.15}FA_{0.85}SnI_3$ perovskites.

To further explore the energy level which is more reflective of the actual ETM layer in PSCs, we fabricated the films of ETMs onto the surface of ITO, which were used for the CV measurements in acetonitrile (Fig. 2c). The LUMO levels for the spin-coated PCBM, OC, and ICBA films were estimated to be −4.14, −3.98, and −3.95 eV based on the E_{onset} (−0.96, −1.12, and −1.15 V), respectively, with the trend aligning closely with the results from the measurements in solution. These results indicate a compatible energy-matching of OC toward the 2D/3D $PEA_{0.15}FA_{0.85}SnI_3$ perovskite (Fig. 2d). This component of the perovskite could afford high V_{OC} for Sn-based PSCs.[11,32] Scanning electronic microscopy (SEM) measurements were performed to examine the morphology of OC, PCBM, and ICBA films on $PEA_{0.15}FA_{0.85}SnI_3$ perovskite layers (Fig. S3, ESI†). These derivatives were fabricated by a mixed solvent[32] of chlorobenzene (CB)/CS_2/1,2,4-trichlorobenzene (TCB) (10/5/1, v/v). They showed similar solubility in this solvent system. The average thickness was *ca.* 40 nm prepared with a precursor solution of 15 mg mL^{-1} with spin coating at 2000 rpm (Fig. S4, ESI†). All the fullerene derivatives showed similar morphologies without discernible pinholes. In the atomic force microscopy (AFM) results (Fig. S5, ESI†), the average root-mean-square (RMS) surface roughness of OC was 5.8 nm, which was comparable to that of PCBM films (6.1 nm) and slightly larger than that of ICBA films (3.6 nm). Together with the SEM observation, these results suggest that the morphology of OC films is similar to those of PCBM and ICBA.

Considering the basicity of the pyridyl group on OC, we checked for protonation by NMR measurement using a mixture of OC and FAI in DMSO-d_6 solution (Fig. S6, ESI†). No peak shift was detected, suggesting that Brønsted–Lowry acid–base reactions are unlikely in the solution.[33] We then carried out X-ray photoelectron spectroscopy (XPS) characterization to check the passivation effect of OC on the Sn-based perovskite layer. Generally, passivation by molecular coordination to the defects, such as undercoordinated ions, would lead to a shift in the XPS peaks.[33,34] The negligible peak shifts in Sn $3d_{5/2}$ and I $3d_{5/2}$ (Fig. S7, ESI†) suggest very limited passivation on the $PEA_{0.15}FA_{0.85}SnI_3$ by OC. Stronger interactions were perhaps inhibited by the steric hindrance from the *tert*-butyl group in OC.

After confirming that OC is suitable to be used as the ETM for Sn-based PSCs in terms of the energy levels and the film-forming ability, we fabricated inverted Sn-based PSCs with the structure ITO/PEDOT:PSS/$PEA_{0.15}FA_{0.85}SnI_3$/OC/BCP/Ag. PEDOT:PSS is poly(3,4-ethylenedioxythiophene):poly(styrenesulfonate) and BCP is bathocuproine (Fig. 3a). Similar devices using PCBM or ICBA as ETMs were fabricated as benchmarks. The current density–voltage (*J*–*V*) curves evaluated under simulated solar illumination

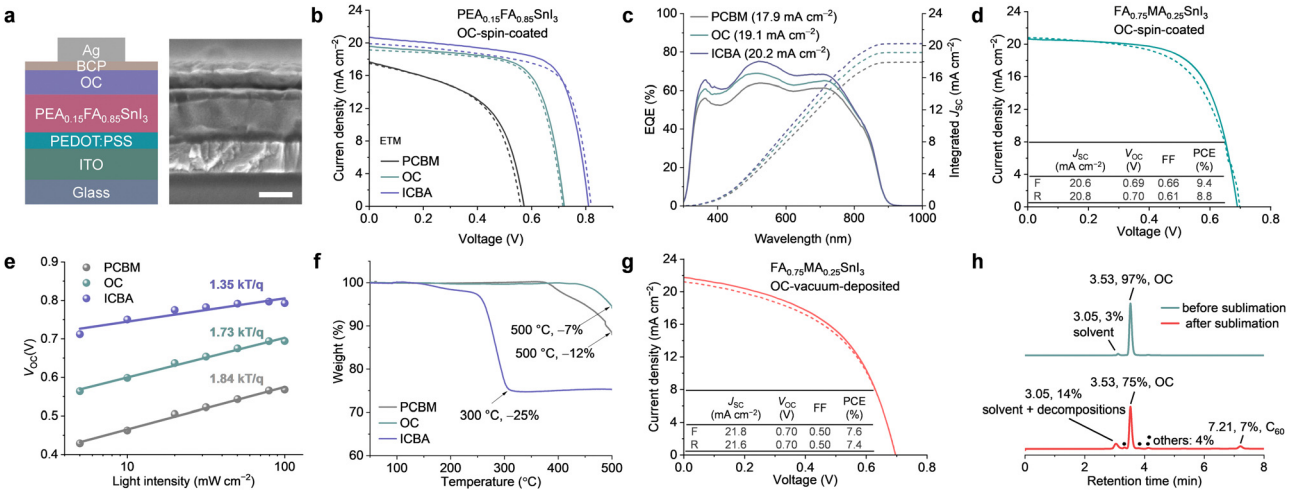

Fig. 3 (a) Schematic illustration and cross-section SEM images of the devices (scale bar is 200 nm). (b) J–V curves of champion devices based on 2D/3D $PEA_{0.15}FA_{0.85}SnI_3$ perovskite with PCBM, OC, and ICBA. Forward (J_{SC} to V_{OC}) and reverse (V_{OC} to J_{SC}), scans are shown with solid and dashed lines, respectively. (c) EQE spectra of the devices with PCBM, OC, and ICBA. (d) J–V curves of champion devices based on 3D $FA_{0.75}MA_{0.25}SnI_3$ perovskite with OC. F and R denote forward and reverse scans, shown with solid and dashed lines, respectively. (e) V_{OC} as a function of illumination intensity for the devices based on PCBM, OC, and ICBA (k is Boltzmann's constant, T is 298 K, and q is the unit of electronic charge). (f) TGA results of PCBM, OC, and ICBA with the weight loss. (g) J–V curves of champion devices (3D $FA_{0.75}MA_{0.25}SnI_3$ perovskite) with OC deposited *via* thermal evaporation. (h) HPLC charts of OC before and after sublimation.

(AM 1.5G, 100 mW cm^{-2}) are shown in Fig. 3b, and the corresponding device parameters are summarized in Table S1 and Fig. S8 (ESI†). The control devices with PCBM as the ETM had a PCE of up to 5.3%, short-circuit current density (J_{SC}) of 17.7 mA cm^{-2}, V_{OC} value of 0.57 V, and fill factor (FF) of 0.52. The ICBA-based device delivered a PCE of up to 11.6% with a J_{SC} of 20.7 mA cm^{-2}, V_{OC} value of 0.82 V, and FF of 0.69. Meanwhile, the OC based device exhibited a PCE of 9.6%, with a J_{SC} of 19.6 mA cm^{-2}, V_{OC} value of 0.72 V, and FF of 0.68. As shown in Fig. 3c, the integrated J_{SC} estimated from external quantum efficiency (EQE) spectra was 17.9, 19.1, and 20.2 mA cm^{-2} for the devices based on PCBM, OC, and ICBA, respectively, in close agreement with the values obtained from the J–V curves. Notably, the trend in the V_{OC} values of the devices (Fig. S8c, ESI†) is consistent with the LUMO levels of the fullerene derivatives. To verify the universality of OC in Sn-based PSCs, we also used OC as the ETM in 3D $FA_{0.75}MA_{0.25}SnI_3$-based PSCs. The devices showed a PCE of 9.4% (J_{SC} = 20.6 mA cm^{-2}, V_{OC} = 0.69 V, and FF = 0.66) (Fig. 3d), which is comparable with the 2D/3D Sn-based PSCs ($PEA_{0.15}FA_{0.85}SnI_3$) described above.

Subsequently, we conducted photoluminescence (PL) and time-resolved photoluminescence (TRPL) measurements. As shown in Fig. S9 (ESI†), the $PEA_{0.15}FA_{0.85}SnI_3$ perovskite film with ICBA on top showed the highest PL intensity and the longest TRPL lifetime, followed by those with OC and PCBM. However, it's hard to differentiate the main origin since the PL quenching within the perovskite/ETL stacking can be introduced by both non-radiative charge carrier recombination and carrier extraction.[35] To gain insight into the carrier recombination behaviour in the devices, we further studied the V_{OC}-light intensity dependence and the electrical impedance spectroscopy (EIS). As all cells adopt the same structures except ETM, the difference in the obtained results would be governed by the recombination loss at the interface between the perovskites and ETMs.[36] The ideality factor (n_{id}) values are 1.84, 1,73, and 1.35 for the $PEA_{0.15}FA_{0.85}SnI_3$ devices using PCBM, OC, and ICBA as ETMs, respectively (Fig. 3e), in line with the V_{OC}s of the solar cells and the EIS results (Fig. S10, ESI†), where the parallel resistance of the solar cell using ICBA as the ETM was maintained at a higher bias voltage than OC and, subsequently, PCBM. These results synergistically confirm the reduced charge recombination in the devices with smaller energy level offset. Notably, the space-charge limited current (SCLC) electron mobility for PCBM, OC, and ICBA is 3.2×10^{-4}, 9.5×10^{-5}, and 2.5×10^{-4} cm^2 V^{-1} s^{-1}, respectively (Fig. S11, ESI†), which do not align with the performance of the resultant solar cells. Therefore, the device performance is mainly governed by the energy level offset at the perovskite/ETM interface.

We also tracked the stability of unencapsulated Sn-based devices stored in the dark in an N_2-filled glovebox under open-circuit conditions. The OC-based devices maintained an average of 93% of their initial PCE for over 50 days of storage. On the contrary, those devices based on PCBM and ICBA retained 84% and 64% after the same storage time (Fig. S12, ESI†).

It is also worth noting that OC exhibits superior thermal stability compared with PCBM and ICBA. The thermogravimetric analysis (TGA) results in Fig. 3f show that OC started to lose weight at 450 °C and retained *ca.* 93% of its original weight (−7%) at 500 °C. For PCBM, it began to deplete its weight at 370 °C and only retained 88% of its original weight (−12%) at 500 °C. In stark contrast, ICBA started to show weight loss at a much lower temperature of 140 °C and experienced a substantial 25% weight loss at 300 °C. Motivated by these results, we attempted to deposit the OC ETM films by

vacuum deposition. This device exhibited a maximum PCE of 7.6%, with J_{SC} of 21.8 mA cm^{-2}, V_{OC} of 0.70 V, and FF of 0.50 (Fig. 3g). This result is a huge leap forward compared with previous results using vacuum-deposited fullerene derivatives as ETMs in PSCs,[37,38] in which PCBM showed severe decomposition during evaporation. The cause of the relatively low FF of 0.50 may have been related to the purity of the sublimed OC. As shown in Fig. 3h, HPLC analysis suggests 75% OC in pure form and 7% C_{60} and 18% unknown impurities (+solvent peak) in the deposited thin films. These impurities likely stem from the partial decomposition of OC during vacuum deposition and may have hindered electron extraction in the devices.

In conclusion, we applied an open-cage bis[60]fulleroid as the ETL in Sn-based PSCs. This compound exhibits a higher LUMO level than PCBM and is comparable to ICBA. The mitigated energy level offset between the Sn-based PSCs and the ETMs results in improved electron extraction and suppressed non-radiative recombination in the devices. Consequently, the devices with OC achieved PCEs of nearly 10% for both 3D and 2D/3D Sn-based PSCs with improved stability. Meanwhile, OC exhibited excellent thermal stability compared with commonly used PCBM and ICBA. Our work addresses the gaps in applying open-cage fullerene derivatives for PSCs. We will continue to design new open-cage fullerene derivatives with shallower LUMO levels and enhanced thermal stability by modifying the aryl groups or transitioning to a higher fullerene, such as C_{70}.

This work was partially supported by JST-Mirai Program (JPMJMI22E2), NEDO, JST SPRING (JPMJSP2110), JSPS KAKENHI Grant Number JP21H04699, JP23H01784 and JP22H04538, The Mazda Foundation, Advanced Technology Institute Research Grants 2023, Nippon Shokubai Award in Synthetic Organic Chemistry, Japan, JACI Prize for Encouraging Young Researcher, the International Collaborative Research Program of ICR, Kyoto University, ICR Grants for Promoting Integrated Research, Kyoto University, and grants for the Integrated Research Consortium on Chemical Sciences. We also thank Prof. Toshiyuki Nohira and Dr Takayuki Yamamoto (Kyoto University) for the XPS measurement and Prof. D. Duan for the purification of the materials (Yunnan University).

Conflicts of interest

A. W. is a co-founder and CSO of EneCoat Technologies, Co., Ltd.

Notes and references

1 Best Research-Cell Efficiency Chart, National Renewable Energy Laboratory, https://www.nrel.gov/pv/cell-efficiency.html.
2 A. Abate, *Joule*, 2017, **1**, 659–664.
3 A. Babayigit, A. Ethirajan, M. Muller and B. Conings, *Nat. Mater.*, 2016, **15**, 247–251.
4 T. Nakamura, Y. Kondo, N. Ohashi, C. Sakamoto, A. Hasegawa, S. Hu, M. A. Truong, R. Murdey, Y. Kanemitsu and A. Wakamiya, *Bull. Chem. Soc. Jpn.*, 2024, uoad025, DOI: 10.1093/bulcsj/uoad025.
5 T. Nakamura, T. Handa, R. Murdey, Y. Kanemitsu and A. Wakamiya, *ACS Appl. Electron. Mater.*, 2020, **2**, 3794–3804.
6 E. Aktas, N. Rajamanickam, J. Pascual, S. Hu, M. H. Aldamasy, D. D. Girolamo, W. Li, G. Nasti, E. Martínez-Ferrero, A. Wakamiya, E. Palomares and A. Abate, *Commun. Mater.*, 2022, **3**, 104.
7 A. Abate, *ACS Energy Lett.*, 2023, **8**, 1896–1899.
8 S. Hu, J. A. Smith, H. J. Snaith and A. Wakamiya, *Precis. Chem.*, 2023, **1**, 69–82.
9 B.-B. Yu, Z. Chen, Y. Zhu, Y. Wang, B. Han, G. Chen, X. Zhang, Z. Du and Z. He, *Adv. Mater.*, 2021, **33**, 2102055.
10 W. Shockley and H. J. Queisser, *J. Appl. Phys.*, 1961, **32**, 510–519.
11 X. Jiang, F. Wang, Q. Wei, H. Li, Y. Shang, W. Zhou, C. Wang, P. Cheng, Q. Chen, L. Chen and Z. Ning, *Nat. Commun.*, 2020, **11**, 1245.
12 Z. Xing, S.-H. Li and S. Yang, *Small Struct.*, 2022, **3**, 2200012.
13 C. Wu, W. Zhu, S. Wang, Z. Cao, L. Ding and F. Hao, *Chem. Commun.*, 2022, **58**, 13007–13010.
14 T. Umeyama and H. Imahori, *Acc. Chem. Res.*, 2019, **52**, 2046–2055.
15 Y. Lin, B. Chen, F. Zhao, X. Zheng, Y. Deng, Y. Shao, Y. Fang, Y. Bai, C. Wang and J. Huang, *Adv. Mater.*, 2017, **29**, 1700607.
16 C. Sun, P. Yang, Z. Nan, C. Tian, Y. Cai, J. Chen, F. Qi, H. Tian, L. Xie, L. Meng and Z. Wei, *Adv. Mater.*, 2023, **35**, 2205603.
17 L. Gan, *Acc. Chem. Res.*, 2019, **52**, 1793–1801.
18 S. Bloodworth and R. J. Whitby, *Commun. Chem.*, 2022, **5**, 121.
19 Y. Hashikawa and Y. Murata, *Bull. Chem. Soc. Jpn.*, 2023, **96**, 943–967.
20 C.-P. Chen, Y.-W. Lin, J.-C. Horng and S.-C. Chuang, *Adv. Energy Mater.*, 2011, **1**, 776–780.
21 C.-P. Chen, C.-Y. Huang and S.-C. Chuang, *Adv. Funct. Mater.*, 2015, **25**, 207–213.
22 C.-M. Hsieh, H.-C. Hsiao, Y. Yamada, W.-R. Wu, U.-S. Jeng, C.-J. Su, Y.-S. Lin, M. Murata, Y. J. Chang and S.-C. Chuang, *ACS Appl. Mater. Interfaces*, 2022, **14**, 39109–39119.
23 E. Castro, A. Artigas, A. Pla-Quintana, A. Roglans, F. Liu, F. Perez, A. Lledó, X.-Y. Zhu and L. Echegoyen, *Materials*, 2019, **12**, 1314.
24 S. H. Park, C. Yang, S. Cowan, J. K. Lee, F. Wudl, K. Lee and A. J. Heeger, *J. Mater. Chem.*, 2009, **19**, 5624–5628.
25 C. Yang, S. Cho, A. J. Heeger and F. Wudl, *Angew. Chem., Int. Ed.*, 2009, **48**, 1592–1595.
26 T. Nagamachi, Y. Takeda, K. Nakayama and S. Minakata, *Chem. – Eur. J.*, 2012, **18**, 12035–12045.
27 C.-Z. Li, J. Huang, H. Ju, Y. Zang, J. Zhang, J. Zhu, H. Chen and A. K.-Y. Jen, *Adv. Mater.*, 2016, **28**, 7269–7275.
28 C. H. Suresh, P. S. Vijayalakshmi, S.-I. Iwamatsu, S. Murata and N. Koga, *J. Org. Chem.*, 2003, **68**, 3522–3531.
29 Y. Hashikawa and Y. Murata, *Chem. Commun.*, 2023, **59**, 1645–1648.
30 B. Kim, J. Lee, J. H. Seo, F. Wudl, S. H. Park and C. Yang, *J. Mater. Chem.*, 2012, **22**, 22958–22963.
31 K. Kurotobi and Y. Murata, *Science*, 2011, **333**, 613–616.
32 W. Liu, S. Hu, J. Pascual, K. Nakano, R. Murdey, K. Tajima and A. Wakamiya, *ACS Appl. Mater. Interfaces*, 2023, **15**, 32487–32495.
33 S. Hu, P. Zhao, K. Nakano, R. D. J. Oliver, J. Pascual, J. A. Smith, T. Yamada, M. A. Truong, R. Murdey, N. Shioya, T. Hasegawa, M. Ehara, M. B. Johnston, K. Tajima, Y. Kanemitsu, H. J. Snaith and A. Wakamiya, *Adv. Mater.*, 2023, **35**, 2208320.
34 Z. Wu, M. Jiang, Z. Liu, A. Jamshaid, L. K. Ono and Y. Qi, *Adv. Energy Mater.*, 2020, **10**, 1903696.
35 A. Al-Ashouri, E. Köhnen, B. Li, A. Magomedov, H. Hempel, P. Caprioglio, J. A. Márquez, A. B. M. Vilches, E. Kasparavicius, J. A. Smith, N. Phung, D. Menzel, M. Grischek, L. Kegelmann, D. Skroblin, C. Gollwitzer, T. Malinauskas, M. Jošt, G. Matič, B. Rech, R. Schlatmann, M. Topič, L. Korte, A. Abate, B. Stannowski, D. Neher, M. Stolterfoht, T. Unold, V. Getautis and S. Albrecht, *Science*, 2020, **370**, 1300–1309.
36 D. Luo, R. Su, W. Zhang, Q. Gong and R. Zhu, *Nat. Rev. Mater.*, 2020, **5**, 44–60.
37 H. Shibuya, Y. Suk Choi, T. Choi, S. Yun, J. Moon and Y. Matsuo, *Chem. – Asian J.*, 2022, **17**, e202200609.
38 Y. Matsuo, S. Ishikawa, H. Amada, K. Yokoyama, Q.-J. Shui, M. Huda, N. Ueoka and H.-S. Lin, *Chem. Lett.*, 2023, **52**, 685–687.